

Spin polarization of photoelectrons in bichromatic extreme-ultraviolet atomic ionization

E. V. Gryzlova¹, M. M. Popova,^{1,2} and A. N. Grum-Grzhimailo¹

¹*Skobeltsyn Institute of Nuclear Physics, Lomonosov Moscow State University, Moscow 119991, Russia*

²*Faculty of Physics, Lomonosov Moscow State University, Moscow 119991, Russia*



(Received 24 April 2020; accepted 3 November 2020; published 25 November 2020)

Spin polarization of photoelectrons is considered in the ionization of atoms by a laser field and its second harmonic, concentrating on the effects of interference between the two ionization paths. The possibility for a crucial increase of the spin polarization by manipulating the relative phase of the harmonics is demonstrated. Observation of these effects, exemplified by the ionization of neon atoms, is accessible by modern free-electron lasers working in the extreme-ultraviolet wavelength regime.

DOI: [10.1103/PhysRevA.102.053116](https://doi.org/10.1103/PhysRevA.102.053116)

I. INTRODUCTION

The spin of an electron is a property of highest importance in both fundamental science and applications. Generally, every photoinduced electron emission is spin polarized [1]. This phenomenon is used in studies of the magnetic properties of matter [2,3], surfaces and thin films [4], single-molecule magnets [5], topological materials [6], spin-dependent quantum interference [7], photoemission chronoscopy [8,9], as well as in the production of polarized electron beams [10,11], to name just a few. Spin-sensitive photoelectron spectrometry of atoms and molecules in the gas phase provides detailed information on the dynamics of photoionization and Auger decay [12,13]. It is an important attribute of the “complete experiment” to determine all amplitudes related to the process [14–16]. Recently a new incentive for spin measurement appeared in connection with spin-resolved Wigner time-delay [17,18]. Furthermore, spin polarization of photoelectrons in strong-field ionization probes the dynamics of ionization in the tunneling and over-barrier regimes [19–22]. Experimentally, the measurement of spin polarization has always been a challenging endeavor. Due to the generally low efficiency of spin detectors, the required acquisition times are long and limit to some extent the broad application of spin-resolved measurements at synchrotron radiation sources, especially with dilute targets.

Short-wavelength free electron lasers (FELs) have started now to provide intense femtosecond radiation pulses with longitudinal coherence, variable polarization, and intensities high enough to observe nonlinear effects in the extreme ultraviolet (XUV). In particular, coherent control of the photoelectron angular distribution (PAD) in the bichromatic XUV ionization of atomic neon has been demonstrated at FERMI in Trieste (Italy) [23], and this field is growing rapidly [24–27]. Formerly, the coherent control was usually realized by lasers operating in the optical wavelength regime, which can easily be rearranged in phase, wavelength, and polarization.

The concept of coherent control is based on the interference of amplitudes of two or several pathways from an initial state of a system to its final state. By changing the phase

between the amplitudes, the desired result of the process is achieved [28]. In the bichromatic atomic ionization,

$$A + \left\{ \begin{array}{l} \hbar\omega + \hbar\omega \\ \hbar(2\omega) \end{array} \right\} \rightarrow A^+ + e^-, \quad (1)$$

these two reaction pathways are the two-photon ionization at the fundamental frequency (ω) and the one-photon ionization at the second-harmonic frequency (2ω). The two-photon pathway can be enhanced by exciting an intermediate resonance, which brings the signal of both pathways to a similar level. The two-pathway interference in the $(\omega + 2\omega)$ process results in novel features in the PAD [29–34]. For example, the asymmetry of the PAD along the direction of the linear polarization of the FEL was used to demonstrate the phase correlation of the two colors, to manipulate it [23,25], and thereby to characterize completely the phase and amplitude of the bichromatic XUV light [35].

The coherent control of the spin in the electron emission from atoms has not been realized experimentally yet. It has been discussed for the $(\omega + 2\omega)$ process with a significant level of abstraction in Refs. [36,37] in the general context of the relationship between classical and quantum interpretations of the coherent control. An experimental evidence of controlling the spin of electronic carriers in semiconductors by bichromatic fields with crossed linear polarizations was detected [38,39], representing a promising effect for creating an ultrafast spin switch in spintronics [40].

In this paper we consider photoelectron spin polarization in the $(\omega + 2\omega)$ process with closed-shell atoms in the XUV, concentrating on the effects of the two-pathway interference. As demonstrated below, additional features, not observed in the single-color case, for example, additional electron-spin components, appear in the $(\omega + 2\omega)$ ionization. The numerical calculations are performed for the Ne atom at frequencies ω in the region of the $2p^6 \rightarrow 2p^5 4s$ resonances.

In the next section we present our theoretical model, which is followed by our results and discussion for linearly and circularly polarized radiation in Secs. III and IV,

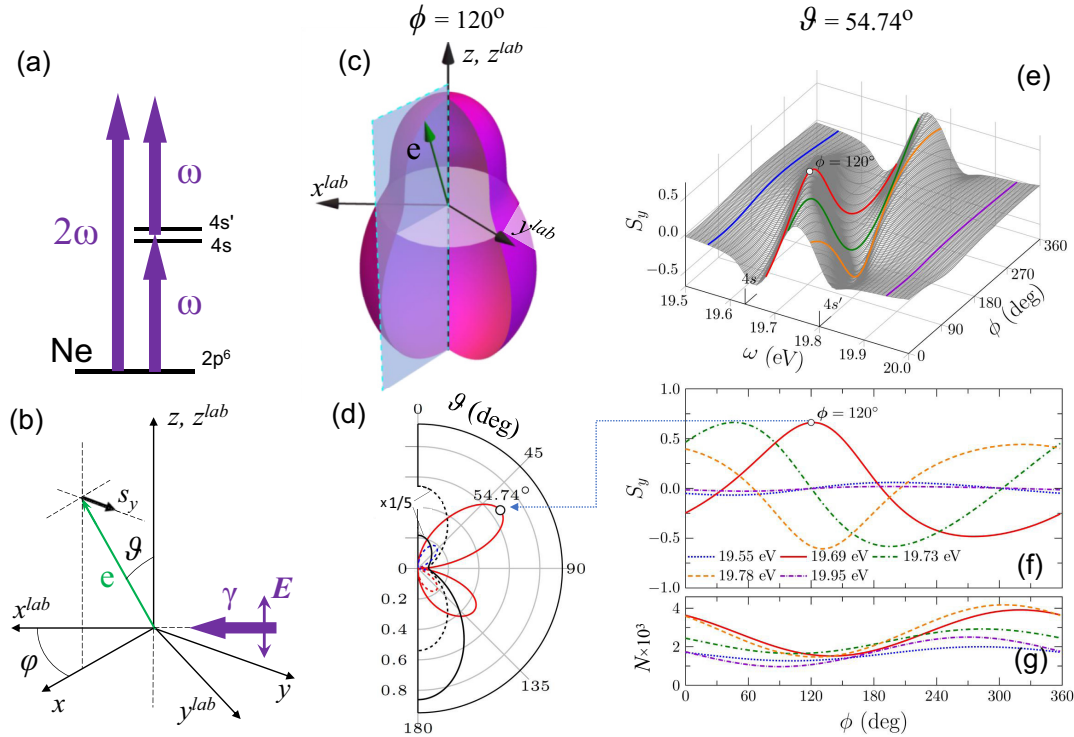


FIG. 1. (a) Scheme of the $(\omega + 2\omega)$ ionization in Ne. (b) Coordinate system. Results for linearly polarized photons: (c) 3D plot of the NPAD, demonstrating axial symmetry with respect to the z axis according to Eq. (4); (d) NPAD and S_y at $\omega = 19.69$ eV and phase $\phi = 120^\circ$ between the harmonics. Curves in panel (d): black - NPAD, red - positive S_y ; blue - negative S_y ; solid - with the two-pathway interference; dashed - without the two-pathway interference; (e) 3D plot of S_y in the region of the $4s$ and $4s'$ resonances as a function of the laser frequency and relative phase of the harmonics. (f) Cuts of the 3D plot in panel (e) at $\omega = 19.55$ eV, $\omega = 19.69$ eV (at the $4s$ resonance), $\omega = 19.73$ eV (between the $4s$ and $4s'$ resonances), $\omega = 19.78$ eV (at the $4s'$ resonance), $\omega = 19.95$ eV. (g) Ionization probability (per pulse per atom), corresponding to the cuts in panel (f). The value of ϕ corresponding to figures in panels (c) and (d) is marked by small circles on the red curves in panels (e) and (f).

respectively. The final section is devoted to the conclusions. Cumbersome formalism is shifted to the Appendix.

II. THEORETICAL MODEL

The lowest nonvanishing order of perturbation theory (LOPT) with respect to the interaction of the radiation field with matter is normally sufficient for the description of photoelectron spin polarization in the XUV in one-, two- and multiphoton ionization [12,41].

Similar to Refs. [23,31,32,42], we consider, as an example, the $(\omega + 2\omega)$ ionization of neon in the region of the intermediate resonance states $2p^5 4s[3/2]_1 \equiv 4s$ (19.69 eV) and $2p^5 4s[1/2]_1 \equiv 4s'$ (19.78 eV) [43], see Fig. 1(a). Therefore, in our numerical illustrations we use a model applicable to light noble gases, which are convenient targets for current experiments with FELs. Below we assume a flat continuum, in the energy far enough from Cooper minima and autoionizing resonances, which allows us to neglect the spin-orbit interaction in the continuum. These conditions are very well fulfilled in our case: The lowest (non-Rydberg) autoionizing state in Ne is at an excitation energy of 45 eV [44] and Cooper minima are absent [45]. Additionally, we assume that the fine-structure components of the final ion $np^5 2P_{\frac{1}{2}, \frac{3}{2}}$ are not resolved. The latter is usually fulfilled for XUV experiments in Ne and Ar. With these approximations, the spin polarization

of photoelectrons vanishes unless a mechanism allows one to distinguish between the different spin states. In our case this mechanism is provided by the spin-orbit interaction, which causes fine-structure energy splitting of the intermediate state resonantly excited by the fundamental frequency in the upper pathway in Eq. (1), while the single-photon 2ω pathway alone cannot produce the spin polarization.

The bichromatic electric field is described by

$$E(t) = F(t) \text{Re}[\sqrt{I_\omega} e_1 e^{-i\omega t} + \sqrt{I_{2\omega}} e_2 e^{-i(2\omega t + \phi)}], \quad (2)$$

where e_1 (e_2) is the unit polarization vector of the first (second) harmonic, ϕ denotes the relative phase between the harmonics. In all numerical examples below the pulse envelope was taken in the form $F(t) = \sin^2 \Omega t$ ($\Omega = \omega/2N$, $0 \leq t \leq 2\pi N/\omega$). The number of optical cycles was set to $N = 500$, which corresponds in our case to a pulse duration of ≈ 120 fs. The ratio of the amplitudes of the harmonics was taken as $I_{2\omega}/I_\omega = 10^{-3}$ with $I_\omega = 10^{12}$ W/cm², preserving the validity of the LOPT [31]. Note that, for heavier atoms, where spin-orbit interaction in the continuum is essential and spin polarized electrons are emitted both in single- and two-photon ionization, the *incoherent* control over the spin polarization is possible through the modulation of the harmonic intensity ratio. Therefore, one of the reasons to limit ourselves to light atoms is to clearly distinguish the coherent control of the

photoelectron spin polarization due to changing the relative phase between the amplitudes of the two pathways in process (1).

In the LOPT, the ionization amplitude is a sum $U = U^{(1)} + U^{(2)}$, where $U^{(1)}$ ($U^{(2)}$) is the first-order (second-order) amplitude of ionization by the second (first) harmonic. Expanding $U^{(1)}$ and $U^{(2)}$ in terms of partial-wave amplitudes (A5), (A6) proceeds as described in Refs. [31,32] in the long-wave dipole approximation with further expressing the observable quantities in terms of the bilinear combinations of the partial amplitudes. Some details of the formalism is presented in the Appendix. Note that all parametric formulas below remain valid for arbitrary (initially unpolarized) atoms, while particular expressions in the Appendix are obtained within the above described approximations.

The atom (ion) is described in the multiconfigurational Hartree-Fock (MCHF) approximation in the intermediate angular-momentum coupling scheme with mixing coefficients obtained by diagonalization of the Breit-Pauli Hamiltonian [46]. The term-dependent photoelectron wave functions were calculated in the frozen-core Hartree-Fock approximation. In the second-order amplitude, all essential intermediate states ($2p^5 3s[3/2]_1$, $2p^5 3s[1/2]_1$, $2p^5 4s[3/2]_1$, $2p^5 4s[1/2]_1$, $2p^5 3d[3/2]_1$, $2p^5 3d[3/2]_1$, $2p^5 3d[1/2]_1$) with total angular momentum $J = 1$ were taken into account. In our model, spin polarization arises as result of fine-structure splitting, which is important in the vicinity of intermediate resonances. Outside of this small region of frequencies, the spin polarization of the electrons vanishes. It results in a faster convergence of the spin polarization with respect to inclusion of additional intermediate states, compared with calculations of PADs [31,32].

Further analysis is carried out separately for linear and circular polarization.

III. LINEARLY POLARIZED RADIATION

In the photoionization by a linearly polarized beam, $\mathbf{e}_1 = \mathbf{e}_2 \equiv \mathbf{e} = \mathbf{e}^*$ in Eq. (2). Figure 1(b) shows the corresponding geometry. The spin polarization can be derived in the form

$$S_y(\vartheta) = [W(\vartheta)]^{-1} \sin \vartheta \sum_{k=1}^4 p_k \cos^{k-1} \vartheta, \quad (3)$$

where ϑ is the electron emission direction with respect to the electric field of the radiation, p_k are real parameters expressed in terms of bilinear combinations of the partial-wave components, see Eqs. (B13)–(B16) of the Appendix. For convenience we introduced the normalized dimensionless photoelectron angular distribution (NPAD)

$$W(\vartheta) = 1 + \sum_{k=1}^4 \beta_k P_k(\cos \vartheta), \quad (4)$$

where β_k are anisotropy parameters, Eqs. (B9)–(B12). Figure 1(c) shows a three-dimensional (3D) plot of the NPAD, which is characterized by a strong asymmetry due to the two-pathway interference. The spin polarization is normal to the reaction plane, spanned by the electric-field vector and the direction of electron emission, and preserves axial symmetry with respect to the electric vector. This is similar to

the general case of separate one- and two-photon ionization [47,48]. Figure 1(d) shows S_y , Eq. (3), and NPAD, Eq. (4), as a function of ϑ for a selected value of the relative phase $\phi = 120^\circ$ between the harmonics. New features of the spin polarization and the possibility of its coherent control are related to the terms with $k = \text{odd}$ in Eqs. (3) and (4), which represent the contribution of the two-pathway interference in process (1). Qualitatively, these terms violate the symmetry with respect to the plane perpendicular to the electric field and, therefore, give nonzero spin polarization for electrons emitted in this plane. High values of the spin polarization are predicted near to the maxima of the ionization probability as a function of the relative phase of the harmonics ϕ [Figs. 1(e)–1(g)]. For example, S_y may reach the value of 0.7 for the photon energy at the $4s$ resonance at $\phi = 120^\circ$ in comparison with a value of $S_y < 0.2$ without the two-pathway interference (independent of ϕ). Thus, a very efficient coherent control of the photoelectron spin is predicted. It follows from Eq. (3) that terms with $k = \text{even}$ for ϑ and $\pi - \vartheta$ have equal absolute values with the opposite signs, while terms with $k = \text{odd}$ have the same sign. Therefore, detectors placed at ϑ and $\pi - \vartheta$ allow us to separate the two-pathway interference effects on the spin polarization.

IV. CIRCULARLY POLARIZED RADIATION

For circularly polarized beams, we select cases with fixed positive chirality of the fundamental, $\mathbf{e}_1 = -(\mathbf{e}_x + i\mathbf{e}_y)/\sqrt{2}$, and variable, i.e., equal and opposite, chirality of the second harmonic, $\mathbf{e}_2 = \mp(\mathbf{e}_x \pm i\mathbf{e}_y)/\sqrt{2}$, where \mathbf{e}_x (\mathbf{e}_y) is the unit vector along the x^{lab} (y^{lab}) axis. To clearly separate the effects of interference between the two ionization paths in Eq. (1), we first write down the NPAD and the components of the spin polarization for incoherent harmonics:

$$W^0(\vartheta) = 1 + \sum_{k=2,4} \beta_k^0 P_k(\cos \vartheta), \quad (5)$$

$$s_z^0(\vartheta) = z_0 + \sum_{k=2,4} z_k P_k(\cos \vartheta), \quad (6)$$

$$s_x^0(\vartheta) = \sin 2\vartheta (\varepsilon_x + \zeta_x \sin^2 \vartheta), \quad (7)$$

$$s_y^0(\vartheta) = \sin 2\vartheta (\varepsilon_y + \zeta_y \sin^2 \vartheta), \quad (8)$$

where the angle ϑ is counted from the propagation direction of the photon beam ($z \parallel \mathbf{k}$) and superscript “0” indicates the incoherent harmonics. The zx plane, rotating around the z axis, is spanned by the directions of the photon beams and the linear momentum of the electron [Fig. 2(a)]. In Eqs. (5)–(8), β_k^0 [32] and $z_{0,2,4}$, $\varepsilon_{x,y}$, $\zeta_{x,y}$ are model-dependent dynamical parameters, expressed by Eqs. (C7)–(C15). Both NPAD and spin components possess axial symmetry with respect to the photon beam propagation.

In the case of coherent harmonics with opposite helicity, the NPAD and the components of spin polarization are described by the equations

$$W^-(\vartheta, \varphi) = W^0(\vartheta) + \beta_3^- \sin^3 \vartheta \cos(3\varphi - \psi_3^-), \quad (9)$$

$$S_v^-(\vartheta, \varphi) = [W^-(\vartheta, \varphi)]^{-1} [s_v^0(\vartheta) + s_v^-(\vartheta, \varphi)], \quad (10)$$

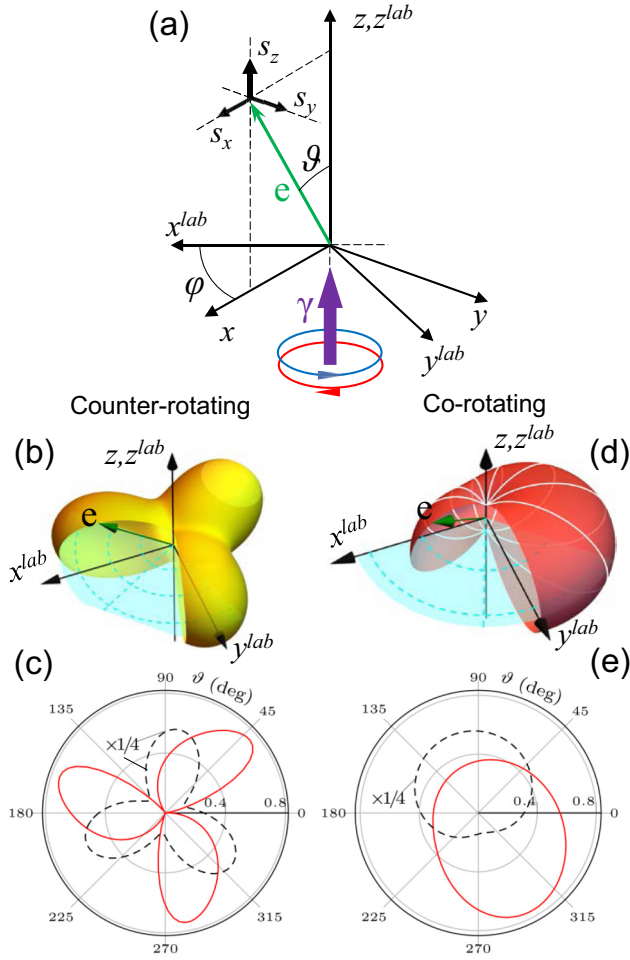


FIG. 2. Results for circularly polarized photons at $\omega = 19.69$ eV (at the $4s$ resonance). (a) Coordinate system, (b) NPAD, (c) NPAD (dashed) and S_z^- (solid) in the plane perpendicular to the beam ($\vartheta = 90^\circ$) for counter-rotating harmonics. Panels (d) and (e) show the same as panels (b) and (c) for corotating harmonics. Zero angle in panels (c) and (e) corresponds to $t = 0$ and $\phi = 0$ in Eq. (2).

where $\nu = x, y, z$ and

$$s_z^-(\vartheta, \varphi) = 2\gamma^- \sin^3 \vartheta \cos(3\varphi - \xi^-), \quad (11)$$

$$s_x^-(\vartheta, \varphi) = -\gamma^- \sin 2\vartheta \sin \vartheta \cos(3\varphi - \xi^-), \quad (12)$$

$$s_y^-(\vartheta, \varphi) = \gamma^- \sin 2\vartheta \sin \vartheta \sin(3\varphi - \xi^-). \quad (13)$$

The superscript “-” indicates opposite helicity and $\gamma^-, \xi^-, \beta_k^-, \psi_k^-$ ($k = 3$) are dynamical parameters (C20), (C21).

The detailed analysis of equations (9)–(13) allows us to draw the following conclusions: (a) The spin components as functions of the azimuthal angle φ of the electron emission show three lobes, like the angular distribution of the emission [32] [Figs. 2(b) and 2(c)] following the total electric-field vector. (b) The two-pathway interference contribution into all components of the spin polarization is described by only one additional term and two real parameters, γ^- and ξ^- . A close inspection shows that this is dictated by conservation of the total angular momentum and its projection [see Eqs. (C16) and (C21)]. (c) The influence of the two-pathway interference

on the s_z^- component (11) is maximal in the plane perpendicular to the beam ($\vartheta = 90^\circ$), where the cross section (9) is also maximal [see, for example, Fig. 2(b) [32] for more detail]. The degree of spin polarization along the beam can reach a value of about 0.75, depending on φ [Fig. 2(c)], in contrast with the constant value of $s_z^0 \approx 0.4$, which is obtained without the two-pathway interference for both chiralities [not shown in Figs. 2(c) and 2(e)]. (d) Variation of the phase ϕ between the harmonics causes the rotation of the patterns described by Eqs. (9)–(13) around the direction of the beams [see Eqs. (C17)–(C19) and the comment after them]. (e) Maximal contributions of the two-pathway interference into the spin components normal to the beams, Eqs. (12) and (13), are observed at the polar “magic angle” of the electron emission $\vartheta = 54.74^\circ$. In our calculations it reaches $+0.35$ for s_x^- and $+0.25$ for s_y^- . (f) The rotation of (11) and (12) around the y axis by the angle ϑ shows that the spin component along the electron emission is not influenced by the two-pathway interference: $s_z^-(\vartheta, \varphi) \cos \vartheta + s_x^-(\vartheta, \varphi) \sin \vartheta = 0$.

For the case of equal helicities, the NPAD and the spin components of the photoelectrons are described by the expressions

$$W^+(\vartheta, \varphi) = W^0(\vartheta) + \sum_{k=1,3} \beta_k^+ \sin^k \vartheta \cos(\varphi - \psi_k^+), \quad (14)$$

$$S_v^+(\vartheta, \varphi) = [W^+(\vartheta, \varphi)]^{-1} [s_v^0(\vartheta) + s_v^+(\vartheta, \varphi)], \quad (15)$$

where the superscript “+” indicates equal helicities,

$$s_z^+(\vartheta, \varphi) = -2\gamma^+ \sin^3 \vartheta \cos(\varphi - \xi^+) + \kappa \sin \vartheta \cos(\varphi - \chi), \quad (16)$$

$$s_x^+(\vartheta, \varphi) = \gamma^+ \sin 2\vartheta \sin \vartheta \cos(\varphi - \xi^+) + \eta \cos \vartheta \cos(\varphi - \delta), \quad (17)$$

$$s_y^+(\vartheta, \varphi) = -\gamma^+ \sin 2\vartheta \sin \vartheta \sin(\varphi - \xi^+) - \eta \cos \vartheta \sin(\varphi - \delta). \quad (18)$$

The contribution of the two-pathway interference is determined in Eqs. (16)–(18) by eight dynamical parameters $\kappa, \chi, \delta, \eta, \gamma^\pm, \xi^\pm$, given by Eqs. (C25)–(C29), with two of them (γ^- and ξ^-) determining the components $s_{x,y,z}^-$, see Eqs. (11)–(13).

The NPAD shows a pattern with one lobe as a function of φ [Figs. 2(d) and 2(e)], while the spin components may change sign, as demonstrated in Fig. 3. The maximal influence of the two-pathway interference on the S_z^+ component is expected for electron emission perpendicular to the beam [Fig. 2(e)]. The spin components S_x^+ and S_y^+ normal to the radiation beam and shown in Fig. 3 possess an interesting feature, specific for the case of equal helicities and illustrated on top of Fig. 3. Namely, the normal component $S_\perp^+ = \{S_x^+, S_y^+\}$ contains the contribution $s_\perp^+ = \{s_x^+, s_y^+\}$ from the two-pathway interference (green arrows in Fig. 3), which is oriented at an almost fixed direction in the laboratory system upon varying the azimuth angle φ of the electron emission. At the same time, $s_\perp^0 = \{s_x^0, s_y^0\}$ strictly follows the azimuthal direction of the electron emission. Therefore, integrating S_\perp^+ over either the entire upper ($0^\circ \leq \vartheta \leq 90^\circ$) or lower ($90^\circ \leq \vartheta \leq 180^\circ$)

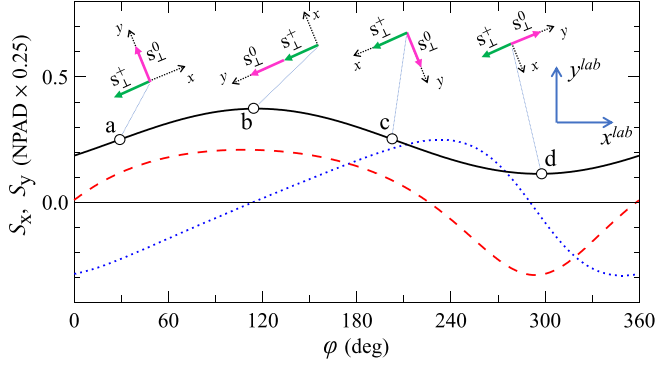


FIG. 3. Spin components S_x^+ (dotted), S_y^+ (dashed), and NPAD (solid) as a function of φ at $\vartheta = 54.74^\circ$ for the relative phase $\phi = 0$ of the corotating fields. (top) Normal to the beam spin components due to the two-pathway interference, s_\perp^+ , and for incoherent harmonics, s_\perp^0 , are shown in the laboratory system $\{x^{\text{lab}}, y^{\text{lab}}\}$ at selected angles φ of the electron emission. The component S_y^+ reaches maximum absolute values at points b and d.

half eliminates the contribution from independent ω and 2ω ionization, leaving only the contribution from their interference. This makes observation of the spin polarization due to the two-pathway interference more affordable.

Our calculations show that some of the parameters in Eqs. (3), (11)–(13), (16)–(18) are very small. To find the origin of this, consider a simplified model neglecting the contribution from the $2p^5 3d$ intermediate states and the term-dependence of the electron wave functions in the continuum $2p^5 \varepsilon l^{2S+1} L$. In this approximation, the two-photon ionization proceeds into a p wave and sums in (B3), (B6), (C3), and (C16) over total and orbital angular momentum J and L can be taken analytically. In this single-configuration approximation, one can obtain equalities $p_1 = p_2 = p_4 = 0$ in Eq. (3), $\eta = 0$, $\gamma^+ = \gamma^-$, $\xi^+ = \xi^-$ in Eqs. (11)–(13) and (16)–(18), and $\varepsilon_x = \varepsilon_y = \zeta_x = \zeta_y = 0$ in Eqs. (7) and (8). Thus, in this simple model, the spin polarization for linearly polarized field as well as any spin component normal to the field propagation for circularly polarized field, is the result of the two-pathway interference.

V. CONCLUSION

The advent of high brilliant seeded FELs and recent progress in electron-spin-sensitive detectors [49,50] make spin-resolved measurements in the XUV feasible in the $(\omega + 2\omega)$ arrangement. We predict and back up with numerical calculations some new features of the spin polarization of electron emission in the bichromatic $(\omega + 2\omega)$ ionization by linearly and circularly polarized radiation. Interference between the one-photon and two-photon ionization pathways leads to new spin components and crucially changes other components. In the example of neon, efficient coherent control of spin polarization is predicted in the XUV in the region of excited atomic states.

ACKNOWLEDGMENTS

The authors benefited greatly from stimulating discussions with Michael Meyer, Klaus Bartschat, and Markus Drescher. E.V.G. and M.M.P. acknowledge support from the Foundation for the Advancement of Theoretical Physics and Mathematics BASIS via the Junior Leader program.

APPENDIX A: DEFINITIONS

Our approach is based on statistical tensor formalism [51,52]. The statistical tensor of spin $\frac{1}{2}$ is defined as

$$\rho_{c\gamma} \left(\frac{1}{2}, \frac{1}{2} \right) = \sum_{\mu\mu'} (-1)^{\frac{1}{2}-\mu'} \left(\frac{1}{2}\mu, \frac{1}{2} - \mu' \mid c\gamma \right) \left(\frac{1}{2}\mu \mid \rho \mid \frac{1}{2}\mu' \right), \quad (\text{A1})$$

where μ (μ') is the spin projection, $\langle \frac{1}{2}\mu \mid \rho \mid \frac{1}{2}\mu' \rangle$ is the spin density matrix, and standard notation for the Clebsch-Gordan coefficient is used. Below we abbreviate $\rho_{c\gamma} \equiv \rho_{c\gamma}(\frac{1}{2}, \frac{1}{2})$. The tensor components ρ_{00} and ρ_{10} are real and $\rho_{11} = -\rho_{1-1}^*$. The Cartesian components of electron-spin polarization are related to the statistical tensors (A1) (given in the same coordinate system):

$$S_z = 2\rho_{10}/\rho_{00}, \quad (\text{A2})$$

$$S_x = -\sqrt{2}(\rho_{11} - \rho_{1-1})/\rho_{00}, \quad (\text{A3})$$

$$S_y = -i\sqrt{2}(\rho_{11} + \rho_{1-1})/\rho_{00}. \quad (\text{A4})$$

Because we intrusted in dimensionless parameters of angular anisotropy and spin polarization, we do not normalize the density matrix and its trace is proportional to the ionization probability.

Following the approach of Refs. [31,32] we introduce similar brief notations for the reduced amplitudes of single- and two-photon ionization, respectively:

$$D_l \equiv e^{i\Delta_l^{(1)}} T^{(1)} D_{0 \rightarrow L_f l, 1}^{(0)}, \quad (\text{A5})$$

$$\begin{aligned} D_{lLJ} & \equiv e^{i\Delta_l^{(2)}} \left(\sum_{nL_n} \alpha_{10}^{\zeta_n^*} \alpha_{L_n S}^{\zeta_n} T_{E_n}^{(2)} \left\{ \begin{matrix} S & L & J \\ 1 & 1 & L_n \end{matrix} \right\} D_{0 \rightarrow n, 1}^{(0)} D_{n, L_n \rightarrow L_f l, L}^{(S)} \right). \end{aligned} \quad (\text{A6})$$

Here l is the orbital momentum of the electron, $e^{i\Delta_l^{(1)}} \equiv -i^{-l} e^{i\delta_l}$, $e^{i\Delta_l^{(2)}} \equiv -i^{-l} e^{i\delta_l}$ with δ_l being the scattering phase in the photoionization channel with orbital angular momentum l , L_f is the orbital angular momentum of the final ion, S , L , J are spin, orbital and total angular momenta of the system “ion + electron,” respectively. The value of S is indicated in parentheses in the superscript of D and “0” in its subscript denotes the ground state of a closed-shell atom. It is implied that the intermediate state is described by the wave function of the form

$$\mid \zeta_n J_n \rangle = \sum_{L_n S_n} \alpha_{L_n S_n}^{\zeta_n} \mid \zeta_n L_n S_n J_n \rangle, \quad (\text{A7})$$

where L_n , S_n , and J_n are orbital, spin, and total angular momenta of the intermediate state with the energy E_n ,

respectively, and ζ_n is a set of quantum numbers that may be needed to further identify this state. Here and below the standard notations for the Wigner nj symbols are used, and

$$D_{0 \rightarrow L_f l, 1}^{(0)} \equiv \langle \zeta_f L_f l : L = 1 || D || 0 \rangle, \quad (\text{A8})$$

$$D_{n, L_n \rightarrow L_f l, L}^{(S)} \equiv \langle \zeta_f L_f l : L || D^S || \zeta_n L_n \rangle \quad (\text{A9})$$

are the reduced dipole matrix elements. The time factors, which depend on the pulse parameters, are given by

$$T^{(1)} = \kappa_1 F_0 e^{-i\phi} \int_0^{NT} \sin^2(\Omega t') e^{i(E - E_0 - 2\omega t')} dt', \quad (\text{A10})$$

$$T_{E_n}^{(2)} = \kappa_2 F_0^2 \int_0^{NT} \sin^2(\Omega t') e^{i(E - E_n - \omega)t'} \times \int_0^{t'} \sin^2(\Omega t'') e^{i(E_n - E_0 - \omega)t''} dt'', \quad (\text{A11})$$

where E is the electron energy and E_0 is the energy of the initial state. $\kappa_1 = 1/\sqrt{2}$ for right-polarized (left-polarized) second harmonic, and $\kappa_1 = 1/2$ for the linearly polarized harmonic. $\kappa_2 = 1/2$ and $\kappa_2 = 1/4$ for circularly and linearly polarized fundamental, respectively.

Components of statistical tensors of the electron spin, as a function of the electron emission angle, can be expanded in terms of spherical harmonics. We write it down in the coordinate system xyz , associated with the electron emission, see Figs. 1(b) and 2(a):

$$\rho_{c\gamma} = \sum_{kqd} (kq, c\gamma | dq + \gamma) B[k, c, d] Y_{kq}(\vartheta, \varphi) e^{i\gamma\varphi}, \quad (\text{A12})$$

where $Y_{kq}(\theta, \varphi)$ is the spherical harmonic, angles θ, φ determine the direction of the electron emission. We use this coordinate system throughout the whole Appendix. $B[k, c, d]$ are dynamical parameters, independent of the coordinate system. It is convenient to separate the statistical tensor into three parts, corresponding to contributions from single-photon ionization by the second harmonic $\rho^{2\omega}$, two-photon ionization by the fundamental harmonic ρ^ω , and the interference part $\rho^{\omega, 2\omega}$:

$$\rho_{c\gamma} = \rho_{c\gamma}^{2\omega} + \rho_{c\gamma}^\omega + \rho_{c\gamma}^{\omega, 2\omega}. \quad (\text{A13})$$

Omitting laborious but straightforward derivations in the spirit of Refs. [31,32] we present below a list of expressions for the dynamical parameters for the particular polarization of photons together with expressions for the electron angular anisotropy and spin-polarization parameters.

APPENDIX B: LINEARLY POLARIZED PHOTONS

The dynamical parameters for single-photon ionization are expressed as

$$B^{2\omega}[k, 0, k] = \frac{1}{\sqrt{2}} \sum_{l'l} \hat{l}l'(l0, l'0 | k0)(10, 1 - 0 | k0) \times \begin{Bmatrix} l & l' & k \\ 1 & 1 & L_f \end{Bmatrix} D_l D_{l'}^*, \quad (\text{B1})$$

where $\hat{a} = \sqrt{2a+1}$. The dynamical parameters (B1) are real and only the scalar component of the spin statistical tensor is

nonvanishing:

$$\rho_{00}^{2\omega} = \sum_{k=0,2} B^{2\omega}[k, 0, k] \hat{k}^{-1} Y_{k0}(\vartheta, \varphi). \quad (\text{B2})$$

For the two-photon ionization,

$$B^\omega[k, c, d] = \sum_{\substack{l'l'j'j' \\ ll'ss'}} (-1)^{S'+L'+k+c} \hat{k} \hat{l} \hat{l}' \hat{L} \hat{L}' \hat{S} \hat{S}' \hat{J} \hat{J}' \times (l0, l'0 | k0)(J0, J'0 | d0)(10, 10 | J0) \times (10, 10 | J'0) \begin{Bmatrix} L & L' & k \\ l' & l & L_f \end{Bmatrix} \begin{Bmatrix} \frac{1}{2} & \frac{1}{2} & c \\ S' & S & S_f \end{Bmatrix} \times \begin{Bmatrix} S & J & L \\ S' & J' & L' \\ c & d & k \end{Bmatrix} D_{lLJ} D_{l'L'J'}^*, \quad (\text{B3})$$

where S_f is the spin of the final ion. Because of the properties of the Clebsch-Gordan coefficients both k and y are even, and therefore $\rho_{10}^\omega = 0$. Other components of the electron spin statistical tensor can be derived as

$$\rho_{00}^\omega = \sum_{k=0,2,4} B^\omega[k, 0, k] \hat{k}^{-1} Y_{k0}(\vartheta, \varphi), \quad (\text{B4})$$

$$\rho_{11}^\omega = \sum_{k,d=0,2,4} (k-1, 11 | d0) B^\omega[k, 1, d] \hat{k}^{-1} Y_{k-1}(\vartheta, \varphi) e^{i\varphi}, \quad (\text{B5})$$

where $B^\omega[k, c, d] = (-1)^{(k+c+d)} B^{\omega*}[k, c, d]$ and are either real ($c = 0$) or imaginary ($c = 1$).

For the interference between single- and two-photon ionization,

$$B^{\omega, 2\omega}[k, c, d] = \frac{1}{\sqrt{2}} \sum_{l'l'L'J'} (-1)^c \hat{k} \hat{l} \hat{l}' \hat{L}' \hat{J}' (l0, l'0 | k0) \times (J'0, 10 | d0)(10, 10 | J'0) \times \begin{Bmatrix} l & l' & k \\ L' & 1 & L_f \end{Bmatrix} \begin{Bmatrix} d & k & c \\ L' & J' & 1 \end{Bmatrix} D_l D_{l'L'J'}^*, \quad (\text{B6})$$

and $B^{\omega, 2\omega}[k, c, d] = (-1)^{(k+c+d)} (B^{2\omega, \omega}[k, c, d])^*$. Both k and d are odd and therefore $\rho_{10}^{\omega, 2\omega} = 0$. Other components of the statistical tensors are

$$\rho_{00}^{\omega, 2\omega} = \sum_{k=1,3} (B^{\omega, 2\omega}[k, 0, k] + B^{2\omega, \omega}[k, 0, k]) \hat{k}^{-1} Y_{k0}(\vartheta, \varphi), \quad (\text{B7})$$

$$\rho_{11}^{\omega, 2\omega} = \sum_{kd=1,3} (B^{\omega, 2\omega}[k, 1, d] + B^{2\omega, \omega}[k, 1, d]) \times (k-1, 11 | d0) \hat{k}^{-1} Y_{k-1}(\vartheta, \varphi) e^{i\varphi}. \quad (\text{B8})$$

Furthermore, the angular anisotropy parameters

$$\beta_2 = \mathcal{B}^\omega[2, 0, 2] + \mathcal{B}^{2\omega}[2, 0, 2], \quad (\text{B9})$$

$$\beta_4 = \mathcal{B}^\omega[4, 0, 4], \quad (\text{B10})$$

$$\beta_1 = 2\text{Re}(\mathcal{B}^{\omega, 2\omega}[1, 0, 1]), \quad (\text{B11})$$

$$\beta_3 = 2\text{Re}(\mathcal{B}^{\omega,2\omega}[3, 0, 3]), \quad (\text{B12})$$

and the electron-spin polarization parameters

$$p_2 = \text{Im}\left(-\sqrt{6}\mathcal{B}^{\omega}[2, 1, 2] + \frac{3\sqrt{5}}{2}\mathcal{B}^{\omega}[4, 1, 4]\right), \quad (\text{B13})$$

$$p_4 = -\frac{7\sqrt{5}}{2}\text{Im}(\mathcal{B}^{\omega}[4, 1, 4]), \quad (\text{B14})$$

$$p_1 = \text{Im}(-2\sqrt{2}\mathcal{B}^{\omega,2\omega}[1, 1, 1] + \sqrt{3}\mathcal{B}^{2\omega,\omega}[3, 1, 3]) \quad (\text{B15})$$

$$p_3 = -5\sqrt{3}\text{Im}(\mathcal{B}^{\omega,2\omega}[3, 1, 3]), \quad (\text{B16})$$

where we introduced the dimensionless dynamical parameters

$$\mathcal{B}^a[k, c, d] = \frac{B^a[k, c, d]}{B^\omega[0, 0, 0] + B^{2\omega}[0, 0, 0]}, \quad (\text{B17})$$

with three options for superscript a : $a = \omega$ (for two-photon process), 2ω (for single photon process) and $\omega, 2\omega$ (for the interference term).

APPENDIX C: CIRCULARLY POLARIZED PHOTONS

Denoting $\lambda = \pm 1$ for positive (+) and negative (−) helicity, for the single-photon ionization one obtains

$$B^{2\omega}[k, 0, k] = \frac{1}{\sqrt{2}} \sum_{l'l'} \hat{l}'(l0, l'0 | k0) \\ \times (1\lambda, 1 - \lambda | k0) \begin{Bmatrix} l & l' & k \\ 1 & 1 & L_f \end{Bmatrix} D_l D_{l'}^*. \quad (\text{C1})$$

Similar to the linearly polarized photon, the dynamical parameters (C1) are real and only the scalar component of the statistical tensor is nonvanishing:

$$\rho_{00}^{2\omega} = \sum_{k=0,2} B^{2\omega}[k, 0, k] \hat{k}^{-1} Y_{k0}(\vartheta, \varphi), \quad (\text{C2})$$

where now the dynamical parameter is given by (C1). For the circularly polarized fundamental, only $J = J' = 2$ channels are allowed. The dynamical parameters and the spin statistical tensors take the form

$$B^\omega[k, c, d] = 5 \sum_{\substack{l'l' \\ LL'SS'}} (-1)^{S'+L'+k+c} \hat{k} \hat{c} \hat{l}' \hat{L} \hat{L}' \hat{S} \hat{S}' \\ \times (l0, l'0 | k0)(22, 2 - 2 | d0) \begin{Bmatrix} L & L' & k \\ l' & l & L_f \end{Bmatrix} \\ \times \begin{Bmatrix} \frac{1}{2} & \frac{1}{2} & c \\ S' & S & S_f \end{Bmatrix} \begin{Bmatrix} S & 2 & L \\ S' & 2 & L' \\ c & d & k \end{Bmatrix} D_{lL2} D_{l'L2}^*, \quad (\text{C3})$$

$$\rho_{00}^\omega = \sum_{k=0,2,4} B^\omega[k, 0, k] \hat{k}^{-1} Y_{k0}(\vartheta, \varphi), \quad (\text{C4})$$

$$\rho_{10}^\omega = \sum_{\substack{k=0,2,4 \\ d=1,3}} B^\omega[k, 1, d](k0, 10 | d0) \hat{k}^{-1} Y_{k0}(\vartheta, \varphi), \quad (\text{C5})$$

$$\rho_{11}^\omega = \sum_{\substack{k=0,2,4 \\ d=0,4}} B^\omega[k, 1, d](k - 1, 11 | d0) \hat{k}^{-1} Y_{k-1}(\vartheta, \varphi) e^{i\varphi}. \quad (\text{C6})$$

Similar to linearly polarized photons, $B^\omega[k, c, d] = (-1)^{(k+c+d)}(B^{\omega*}[k, c, d])^*$ and can be either real or imaginary. The nonvanishing angular anisotropy parameters are of the form

$$\beta_2 = \mathcal{B}^\omega[2, 0, 2] + \mathcal{B}^{2\omega}[2, 0, 2], \quad (\text{C7})$$

$$\beta_4 = \mathcal{B}^\omega[4, 0, 4], \quad (\text{C8})$$

where reduced dynamical parameters $\mathcal{B}^a[k, c, d]$ are given by Eq. (B17). The electron-spin polarization parameters are

$$z_0 = 2\mathcal{B}^\omega[0, 1, 1], \quad (\text{C9})$$

$$z_2 = -2\sqrt{\frac{2}{5}}\mathcal{B}^\omega[2, 1, 1] + 2\sqrt{\frac{3}{5}}\mathcal{B}^\omega[2, 1, 3], \quad (\text{C10})$$

$$z_4 = -\frac{4}{3}\mathcal{B}^\omega[4, 1, 3], \quad (\text{C11})$$

$$\varepsilon_x = -\left(\frac{3}{\sqrt{10}}\mathcal{B}^\omega[2, 1, 1] + \sqrt{\frac{3}{5}}\mathcal{B}^\omega[2, 1, 3] + \frac{5}{3}\mathcal{B}^\omega[4, 1, 3]\right), \quad (\text{C12})$$

$$\zeta_x = \frac{35}{12}\mathcal{B}^\omega[4, 1, 3], \quad (\text{C13})$$

$$\varepsilon_y = -\text{Im}\left(\sqrt{\frac{3}{2}}\mathcal{B}^\omega[2, 1, 2] + \sqrt{5}\mathcal{B}^\omega[4, 1, 4]\right), \quad (\text{C14})$$

$$\zeta_y = \frac{7\sqrt{5}}{4}\text{Im}(\mathcal{B}^\omega[4, 1, 4]). \quad (\text{C15})$$

For the interference term,

$$B^{\omega,2\omega}[k, c, d] = \sqrt{\frac{5}{2}} \sum_{l'l'} (-1)^{1+c} \hat{k} \hat{l}' \hat{L}' \\ \times (l0, l'0 | k0)(22, 1 - \lambda | d2 - \lambda) \\ \times \begin{Bmatrix} l & l' & k \\ L' & 1 & L_f \end{Bmatrix} \begin{Bmatrix} d & k & c \\ L' & 2 & 1 \end{Bmatrix} D_l D_{l'L2}^*. \quad (\text{C16})$$

Here we suppose that the fundamental is right polarized ($\lambda = +1$), and the second harmonic is $\lambda = \pm 1$. Thus, Eq. (C16) covers both cases, corotating and counter-rotating beams. The relation $B^{\omega,2\omega}[k, c, d] = (-1)^{(k+c+d+1)}(B^{2\omega,\omega}[k, c, d])^*$ holds and $B^{\omega,2\omega}$ for $\lambda = -1$ is $\sqrt{15}$ times larger than for $\lambda = +1$.

If the helicity of the second harmonic is $\lambda = -1$, i.e., for counter-rotating beams, the spin statistical tensors are of the form

$$\rho_{00}^{\omega,2\omega} = \frac{1}{\sqrt{7}} \{B^{\omega,2\omega}[3, 0, 3]Y_{33}(\vartheta, \varphi) + B^{2\omega,\omega}[3, 0, 3]Y_{3-3}(\vartheta, \varphi)\}, \quad (\text{C17})$$

$$\rho_{10}^{\omega,2\omega} = \frac{\sqrt{3}}{2\sqrt{7}} \{B^{\omega,2\omega}[3, 1, 3]Y_{33}(\vartheta, \varphi) - B^{2\omega,\omega}[3, 1, 3]Y_{3-3}(\vartheta, \varphi)\}, \quad (\text{C18})$$

$$\rho_{11}^{\omega,2\omega} = -\frac{1}{2\sqrt{7}} B^{\omega,2\omega}[3, 1, 3]Y_{32}(\vartheta, \varphi)e^{i\varphi}. \quad (\text{C19})$$

The dynamical parameter (C16) varies with the phase between the harmonics as $\exp[-i\phi]$ [see Eqs. (A5), (A6) and (A10), (A11)] and then from Eqs. (C17)–(C19) it is obvious that PAD and spin polarization rotate with ϕ synchronously. The angular anisotropy and spin-polarization parameters may be written in a short form by two complex equations:

$$\beta_3^- \exp[i\psi_3^-] = -\frac{\sqrt{5}}{2} B^{\omega,2\omega}[3, 0, 3], \quad (\text{C20})$$

$$\gamma^- \exp[i\xi^-] = -\frac{\sqrt{15}}{4} B^{\omega,2\omega}[3, 1, 3]. \quad (\text{C21})$$

For the corotating beams, i.e., for the helicity $\lambda = -1$ of the second harmonic, the components of the spin statistical tensors are of the form

$$\rho_{00}^{\omega,2\omega} = \sum_{k=1,3} \hat{k}^{-1} \{B^{\omega,2\omega}[k, 0, k]Y_{k1}(\vartheta, \varphi) + B^{2\omega,\omega}[k, 0, k]Y_{k-1}(\vartheta, \varphi)\}, \quad (\text{C22})$$

$$\rho_{10}^{\omega,2\omega} = \sum_{\substack{k=1,3 \\ d=1,2,3}} \hat{k}^{-1} (k1, 10 | d1) \{B^{\omega,2\omega}[k, 1, d]Y_{k1}(\vartheta, \varphi) + (-1)^d B^{2\omega,\omega}[k, 1, d]Y_{k-1}(\vartheta, \varphi)\}, \quad (\text{C23})$$

$$\rho_{11}^{\omega,2\omega} = \left(\sum_{\substack{k=1,3 \\ d=1,2,3}} \hat{k}^{-1} (k0, 11 | d1) B^{\omega,2\omega}[k, 1, d]Y_{k0}(\vartheta, \varphi) + \frac{1}{\sqrt{7}} \sum_{d=2,3} (3-2, 11 | d-1) B^{2\omega,\omega}[3, 1, d]Y_{3-2}(\vartheta, \varphi) \right) e^{i\varphi}. \quad (\text{C24})$$

The angular anisotropy and the spin-polarization parameters can be written in the complex form as

$$\beta_1 \exp[i\psi_1] = -\sqrt{2} B^{\omega,2\omega}[1, 0, 1] - 2\sqrt{3} B^{\omega,2\omega}[3, 0, 3], \quad (\text{C25})$$

$$\beta_3 \exp[i\psi_3] = \frac{5\sqrt{3}}{2} B^{\omega,2\omega}[3, 0, 3], \quad (\text{C26})$$

$$\kappa \exp[i\chi] = -2B^{\omega,2\omega}[1, 1, 1] - 2B^{\omega,2\omega}[1, 1, 2] - 2B^{\omega,2\omega}[3, 1, 3] + 8\sqrt{\frac{2}{7}} B^{\omega,2\omega}[3, 1, 2], \quad (\text{C27})$$

$$\gamma^+ \exp[i\xi^+] = -\frac{5}{4} B^{\omega,2\omega}[3, 1, 3] + 5\sqrt{\frac{2}{7}} B^{\omega,2\omega}[3, 1, 2], \quad (\text{C28})$$

$$\eta \exp[i\delta] = 2B^{\omega,2\omega}[1, 1, 1] - 2B^{\omega,2\omega}[1, 1, 2] + \sqrt{2} B^{\omega,2\omega}[3, 1, 3] - 2\sqrt{\frac{2}{7}} B^{\omega,2\omega}[3, 1, 2]. \quad (\text{C29})$$

[1] U. Heinzmann and J. H. Dil, *J. Phys.: Condens. Matter* **24**, 173001 (2012).

[2] H. C. Siegmann, *Phys. Rep.* **17**, 37 (1975).

[3] N. Rougemaille and A. K. Schmid, *Eur. Phys. J.: Appl. Phys.* **50**, 20101 (2010).

[4] P. D. Johnson, *Rep. Prog. Phys.* **60**, 1217 (1997).

[5] A. Helmstedt, N. Dohmeier, N. Müller, A. Gryzia, A. Brechling, U. Heinzmann, V. Hoeke, E. Krickemeyer, T. Glaser, P. Leicht, *et al.*, *J. Electron Spectrosc. Relat. Phenom.* **198**, 12 (2015).

[6] B. Lv, T. Qian, and H. Ding, *Nat. Rev. Phys.* **1**, 609 (2019).

- [7] K. Kuroda, K. Yaji, M. Nakayama, A. Harasawa, Y. Ishida, S. Watanabe, C.-T. Chen, T. Kondo, F. Komori, and S. Shin, *Phys. Rev. B* **94**, 165162 (2016).
- [8] M. Fanciulli, H. Volfová, S. Muff, J. Braun, H. Ebert, J. Minár, U. Heinzmann, and J. H. Dil, *Phys. Rev. Lett.* **118**, 067402 (2017).
- [9] M. Fanciulli and J. H. Dil, *SciPost Phys.* **5**, 058 (2018).
- [10] D. T. Pierce, in *Experimental Methods in the Physical Sciences*, edited by F. B. Dunning and R. G. Hulet (Academic Press, San Diego, 1995), Vol. 29A, p. 1–35.
- [11] L. Cultrera, A. Galdi, J. K. Bae, F. Ikponmwen, J. Maxson, and I. Bazarov, *Phys. Rev. Accel. Beams* **23**, 023401 (2020).
- [12] U. Heinzmann and N. A. Cherepkov, in *VUV and Soft X-ray Photoionization*, edited by U. Becker and D. A. Shirley (Springer US, Boston, 1996), pp. 521–559.
- [13] B. Lonmann, *Angle and Spin Resolved Auger Emission* (Springer, Berlin, Heidelberg, 2009).
- [14] B. Schmidtke, T. Khalil, M. Drescher, N. Müller, N. M. Kabachnik, and U. Heinzmann, *J. Phys. B: At., Mol. Opt. Phys.* **34**, 4293 (2001).
- [15] H. Kleinpoppen, B. Lohmann, and A. N. Grum-Grzhimailo, *Perfect/Complete Scattering Experiments* (Springer, Berlin, Heidelberg, 2013).
- [16] G. Schönhense, K. Medjanik, S. Chernov, D. Kutnyakhov, O. Fedchenko, M. Ellguth, D. Vasilyev, A. Zaporozhchenko-Zymaková, D. Panzer, A. Oelsner, *et al.*, *Ultramicroscopy* **183**, 19 (2017).
- [17] A. Mandal, P. C. Deshmukh, A. S. Kheifets, V. K. Dolmatov, and S. T. Manson, *Phys. Rev. A* **96**, 053407 (2017).
- [18] M. Turconi, L. Barreau, D. Busto, M. Isinger, C. Alexandridi *et al.*, *J. Phys. B: At. Mol. Opt. Phys.* **53**, 184003 (2020).
- [19] I. Barth and O. Smirnova, *Phys. Rev. A* **88**, 013401 (2013).
- [20] D. B. Milosevic, *Phys. Rev. A* **93**, 051402(R) (2016).
- [21] A. Hartung, F. Morales, M. Kunitski, K. Henrichs, A. Laucke, M. Richter, T. Jahnke, A. Kalinin, M. Schöffler, L. Ph. H. Schmidt, *et al.*, *Nat. Photonics* **10**, 526 (2016).
- [22] M.-M. Liu, Y. Shao, M. Han, P. Ge, Y. Deng, C. Wu, Q. Gong, and Y. Liu, *Phys. Rev. Lett.* **120**, 043201 (2018).
- [23] K. C. Prince, E. Allaria, C. Callegari, R. Cucini, G. De Ninno, S. Di Mitri, B. Diviacco, E. Ferrari, P. Finetti, D. Gauthier, *et al.*, *Nat. Photonics* **10**, 176 (2016).
- [24] D. Iablonskyi, K. Ueda, K. L. Ishikawa, A. S. Kheifets, P. Carpeggiani, M. Reduzzi, H. Ahmadi, A. Comby, G. Sansone, T. Csizmadia, *et al.*, *Phys. Rev. Lett.* **119**, 073203 (2017).
- [25] L. Giannessi, E. Allaria, K. C. Prince, C. Callegari, G. Sansone, K. Ueda, T. Morishita, C. N. Liu, A. N. Grum-Grzhimailo, E. V. Gryzlova, *et al.*, *Sci. Rep.* **8**, 7774 (2018).
- [26] D. You, K. Ueda, M. Ruberti, K. L. Ishikawa, P. A. Carpeggiani, C. Tamás, Lénárd Gulyás Oldal, N. G. Harshitha, G. Sansone, P. K. Maroju, *et al.*, *New J. Phys.* **21**, 113036 (2019).
- [27] C. Callegari, A. N. Grum-Grzhimailo, K. L. Ishikawa, K. C. Prince, G. Sansone, and K. Ueda, Atomic, molecular and optical physics applications of longitudinally coherent and narrow bandwidth Free-Electron Lasers (2020), [arXiv:2008.11024](https://arxiv.org/abs/2008.11024).
- [28] M. Shapiro and P. Brumer, *J. Chem. Phys.* **84**, 4103 (1986).
- [29] N. B. Baranova, I. M. Beterov, B. Ya. Zel'dovich, I. I. Ryabtsev, A. N. Chudinov, and A. A. Shul'ginov, *Pis'ma Zh. Eksp. Teor. Fiz.* **55**, 431 (1992) [*JETP Lett.* **55**, 439 (1992)].
- [30] Y.-Y. Yin, C. Chen, D. S. Elliott, and A. V. Smith, *Phys. Rev. Lett.* **69**, 2353 (1992).
- [31] E. V. Gryzlova, A. N. Grum-Grzhimailo, E. I. Staroselskaya, N. Douguet, and K. Bartschat, *Phys. Rev. A* **97**, 013420 (2018).
- [32] E. V. Gryzlova, M. M. Popova, A. N. Grum-Grzhimailo, E. I. Staroselskaya, N. Douguet, and K. Bartschat, *Phys. Rev. A* **100**, 063417 (2019).
- [33] P. V. Demekhin, A. N. Artemyev, A. Kastner, and T. Baumert, *Phys. Rev. Lett.* **121**, 253201 (2018).
- [34] R. E. Goetz, C. P. Koch, and L. Greenman, *Phys. Rev. Lett.* **122**, 013204 (2019).
- [35] M. Di Fraia, O. Plekan, C. Callegari, K. C. Prince, L. Giannessi, E. Allaria, G. Penco, P. R. Ribic, S. Spampinati, C. Spezzani, *et al.*, *Phys. Rev. Lett.* **123**, 213904 (2019).
- [36] T. Scholak and P. Brumer, *J. Chem. Phys.* **141**, 204311 (2014).
- [37] T. Scholak and P. Brumer, *Adv. Chem. Phys.* **162**, 39 (2017).
- [38] M. J. Stevens, A. L. Smirl, R. D. R. Bhat, A. Najmaie, J. E. Sipe, and H. M. van Driel, *Phys. Rev. Lett.* **90**, 136603 (2003).
- [39] J. Hübner, W. W. Rühle, M. Klude, D. Hommel, R. D. R. Bhat, J. E. Sipe, and H. M. van Driel, *Phys. Rev. Lett.* **90**, 216601 (2003).
- [40] D. D. Awschalom, L. C. Bassett, A. S. Dzurak, E. L. Hu, and J. R. Petta, *Science* **339**, 1174 (2013).
- [41] T. Nakajima and P. Lambropoulos, *Europhys. Lett.* **57**, 25 (2002).
- [42] G. M. Nikolopoulos and P. Lambropoulos, *J. Phys. B: At., Mol. Opt. Phys.* **48**, 244006 (2015).
- [43] In the jK -coupling scheme, the $n[K]_j$ indicates, for the Ne atom, that the total angular momentum j of the $2p_j^5$ core is first coupled to the orbital momentum of the excited electron l , $j + l = K$, with subsequent coupling of spin of this electron, $K + s = J$. Primed and not-primed orbitals of the excited electron correspond to $j = \frac{1}{2}$ and $j = \frac{3}{2}$, respectively.
- [44] K. Codling, R. P. Madden, and D. L. Ederer, *Phys. Rev.* **155**, 26 (1967).
- [45] D. J. Kennedy and S. T. Manson, *Phys. Rev. A* **5**, 227 (1972).
- [46] C. F. Fischer, T. Brage, and P. Jönsson, *Computational Atomic Structure. An MCHF Approach* (IOP Publishing, Bristol, 1997).
- [47] N. A. Cherepkov, *J. Phys. B: At. Mol. Phys.* **11**, L435 (1978).
- [48] N. L. Manakov and A. V. Meremianin, *J. Exp. Theor. Phys.* **84**, 1080 (1997).
- [49] G. Schönhense, K. Medjanik, and H. J. Elmers, *J. Electron Spectrosc. Relat. Phenom.* **200**, 94 (2015).
- [50] T. Okuda, *J. Phys.: Condens. Matter* **29**, 483001 (2017).
- [51] S. Devons and L. J. B. Goldfarb, in *Handbuch der Physik. Band 42*, edited by S. Flugge (Springer-Verlag, Berlin, 1957), p. 362.
- [52] V. V. Balashov, A. N. Grum-Grzhimailo, and N. M. Kabachnik, *Polarization and Correlation Phenomena in Atomic Collisions. A Practical Theory Course*, Physics of Atoms and Molecules (Kluwer Academic/Plenum Publishers, New York, Boston, Dordrecht, London, Moscow, 2000).